Solidification and Solid-State Transformation Sciences in Metals Additive Manufacturing

by

Michael M. Kirka[1,2,*], Peeyush Nandwana[1,2], Yousub Lee[1,2], and Ryan R. Dehoff[1,2]
[1]Manufacturing Demonstration Facility, Oak Ridge National Laboratory, Knoxville, TN
[2]Materials Science & Technology Division, Oak Ridge National Laboratory, Oak Ridge, TN

*corresponding author: email: kirkamm@ornl.gov, tel: 1-865-574-1094

Abstract

Additive manufacturing (AM) of metals is rapidly emerging as an established manufacturing process for metal components. Unlike traditional metals fabrication processes, metals fabricated via AM undergo localized thermal cycles during fabrication. As a result, AM presents the opportunity to control the liquid-solid phase transformation, i.e. material texture. However, thermal cycling presents challenges from the standpoint of solid-solid phase transformations. To be discussed are the opportunities and challenges in metals AM in the context of texture control and associated solid-solid phase transformations in Ti-6Al-4V and Inconel 718.

Keywords: Additive Manufacturing, Phase Transformations, Computational Modeling, Superalloys, Titanium Alloys

Much hype has been placed on the ability of metals additive manufacturing (AM) to fabricate objects of unlimited geometric complexity, in a near net shape manner, that makes it impossible for the geometry to be fabricated by traditional means [1]. However, for all the potential metals AM has to offer, serious challenges exist in the form of liquid-solid ($l \rightarrow S$), and solid-solid ($S \rightarrow S$) phase transformations that arise as a result of the thermal gyrations that the material sees during the layer-by-layer fabrication. Furthermore, developing process parameter structure relationships is difficult for non-prismatic geometries due to the complexity of the AM processes. The aim of this paper is to discuss the opportunities and challenges facing metals AM from the perspective of solidification phenomena and phase transformations encountered in Ti-6Al-4V (Ti64) and Inconel 718 (IN718) processed via metals AM. For the purposes of this discussion, the reader is referred to one of the following review articles for detailed discussions on the various AM processes [1] and for a review of phase transformations that occur in Ti64 [2] and IN718 [3].

Overall, the basic fundamental physics of metals AM is identical to that of multi-pass welding whereby a heat source locally melts the material as it passes and then solidifies before being partially melted again on the next pass [4]. However, the key distinguishing differences between welding and metals AM is the complex thermal conditions that arise due to the approximately 27,000 cm of multi-pass weld per cubic centimeter of material fabricated and the numerous process parameters that have the ability to influence thermal conditions locally within a geometry. While in-situ processing methods have the ability to provide thermal information, the information is strictly limited to line of sight, i.e. top surface of a build and do not provide the conditions within the melt pool as the $(l \rightarrow S)$ transformation occur and the layers below that undergo repeated thermal gyrations which can influence the $(S \rightarrow S)$ transformations. Consequently, numerical models are required for understanding the thermal conditions within the melt pool as they relate to texture formation and control.

To understand the effect of melt tracks on the thermal distribution within an AM layer, Hussein et al. [5] implemented a three-dimensional heat transfer model for selective laser melting (SLM). Overlap between melt tracks results in repeated thermal gyrations, with the peak temperature at a material point dropping off towards the background temperature as the heat source moves away as illustrated in Figure 1a. Manvatkar et al. [6] simulated the effects of layer addition (Figure 1b) and observed layer addition results in a reduced cooling rate of the material whereby the solidification front morphology changes from planar to cellular.

Further, modeling attempts have been made to understand the relationship between the thermal conditions related to process and microstructure evolution. Wei et al. [7] performed 3-D heat transfer and fluid mechanics modeling of the melt pool in the SLM process. In their simulation, unidirectional and bidirectional scans were compared to see the effect of scan direction on solidification microstructure of IN718. Unidirectional scans, resulted in primary growth angles aligned with the experimentally observed growth angle. In the case of the bidirectional scans, the model and experiment diverged in the growth angle by 15 °. The discrepancy was attributed to the effect of preferred direction of crystallographic growth for nickel. Helmer et al. [8] showed that by rapidly changing the heat source direction while maintaining a tight overlap between melt tracks a transition from columnar to equiaxed grains can be achieved.

Departing from the traditional linear heat track simulations, Raghavan et al. [9] considered the effect of a point heat source fill on the texture transition between columnar and equiaxed in a controlled manner for the EBM process. Through studying the influence of process parameters on the temperature gradient and solidification rate at the solid-liquid interface, the preheat temperature and beam energy were identified as having the the greatest influence towards controlling the texture within the material.

Experimentally, fabrication of material of a desired texture on a bulk scale requires some trial and

error due to the complex thermal conditions material encounters in AM processes and can only be guided by solidification modeling. Dinda et al. [10] were the earliest to show the ability to influence material texture through scan strategy in the directed energy deposition process was used to manipulate the solidification front and promote the growth of grains at alternating 45° angles with every additional layer. More recently Dehoff et al. [11] demonstrated the ability to control texture in a site-specific manner within IN718 by manipulating the electron beam between a linear heat source to point source to transition between the columnar and equiaxed grain solidification regions as shown in Figure 2. This was demonstrated by forming the letters D, O, and E with equiaxed grains while maintaining columnar grain growth in the remainder of the material. While site-specific microstructure control within structures presents one of the greatest opportunities for AM, the ability to select the necessary processing parameters to result a specific thermal gradient and solidification front velocity in complex geometries is difficult due to the sensitivity of the local thermal conditions to the global thermal conditions in the build.

In what can be considered among the earliest reports on the $S \rightarrow S$ phase transformations observed in Ti64 was by Kobryn and Semiatin [12, 13] in studying Ti64 fabricated by the laser engineered net shape (LENS) process. Observed were elongated columnar β-grains comprised of α laths with a strong fiber texture independent of the incident beam energy utilized. However, associated with this preferred texture and the alignment of lack-of-fusion defects, an anisotropy in the tensile and fatigue properties was reported for the as-fabricated material.

Kelly and Kampe [14] put forth the theory that during laser processing of Ti64 via LENS, α' (hexagonal martensitic phase) forms upon cooling and decomposes into α and β phases over the thermal gyrations associated with multiple passes and layer addition similar to the thermal cycle presented in Figure 1. Theorized was that the melting of a given layer results in the melt pool extending several layers below causing those layers nearest the bottom of the melt pool to see thermal gyrations above the β-transus followed by cooling into the α+β phase field at varying cooling rates. Recently, Sridharan et al. [15] demonstrated the presence of α through the third uppermost layer during DMD processing of Ti64. With additional layers beyond the third, the α' in the first layer was observed to transform to a mixture of colony and basketweave α. Such transformations induce a dominant basal texture with increasing build height during the cooling of the already deposited material from above the β transus [15].

However, the retention of martensitic α' in SLM processed Ti64 has been reported to occur [16, 17]. Simonelli et al. [16] report the absence of α colonies on the grain boundaries in as-fabricated sample as proof of existence of martensite. Whereas Thjis et al. [17] on the other hand reported a mixed microstructure consisting of α' and Ti_3Al phases.The differences between microstructural features in powder-blown vs. powder-bed techniques highlight the role of processing-microstructure relationships that one needs to be cognizant of. Thus, even in the broad spectrum of laser based processing, significant

differences can arise based on the powder delivery technique which would alter the physics of solidification and subsequent phase transformations. Recently Xu et al. [18] demonstrated that the decomposition of α' can be achieved in-situ in SLM by varying parameters such as focal offset distance, layer thickness, and energy density that again highlights the dominant impact of subtle process parameter changes on the final microstructure.

Overall, it is unanimously agreed that the initial cooling rate from β-phase field is greater than 410 $\frac{K}{s}$ such that the formation of α' is facilitated. As more layers are deposited, the initial α' can completely decompose into $\alpha+\beta$ or undergo a partial decomposition according to $\alpha'+\alpha+\beta$ microstructure. As a layer is deposited the phase transformations occurring can be summarized as l$\rightarrow$ $\beta \rightarrow \alpha'$. As more layers are deposited on top of the existing layer, the above-mentioned phase transition occurs with every thermal gyration until the thermal gyration falls into the background temperature. After, that for the next few layers the solid-state phase transformation can cause multiple cycles of diffusionless $\beta \leftrightarrow \alpha'$ depending on the cooling rate. Ideally, the final product should be a mix of α', α, and β phases. Since all laser based processes, powder bed as well as powder blown are carried at room temperature, there is no kinetic and thermodynamic driving force for the complete decomposition of α' without changing process parameters.

Unlike laser AM processes, the high temperatures ($\approx 650°$C) of the EBM process greatly influence the solid-solid phase transformations of Ti64 [19]. Similar to laser based processes, the solidification microstructure involves columnar β grains with a $\langle 001 \rangle$-fiber axis. Various researchers have shown that the final microstructure in EBM fabricated Ti64 is $\alpha + \beta$. Al-Bermani et al. [19] were the first to explain the microstructure formation in EBM fabricated Ti64. They reported that the samples consist of both colony and basketweave $\alpha + \beta$ microstructure and did not observe any variant selection. However, in smaller samples they observed the presence of α' in the top $500\mu m$. Thus, the first transformation is still of the β to α' type. However, as their builds were fabricated in the temperature range of 650-700°C, full decomposition of the martensite was observed.

In an attempt to understand the complex phase transformations occurring, Tan et al. [20] conducted an in-depth study using advanced characterization tools. They reported the presence of a FCC L phase at the α/β interface using TEM as shown in Figures 3a and b and its associated diffraction patterns in the inset. Previously, it was believed that the L phase is a result of formation of titanium hydride during sample preparation [21]. Tan et al. [20] carried out atom probe study to determine the compositional fluctuations at the interface. However, they did not find anything unusual apart from the expected partitioning of α and β stabilizers into the respective phases (Figure 3c). Coupled with the transmission electron microscopy (TEM) results and absence of a hydride phase at the α/β interface they concluded that the L phase is possibly a metastable phase that forms during the decomposition of β to α phase but

the transformation is not completed due to sluggish kinetics at the build temperatures. They also agreed on the initial transformation of β to α' that eventually decomposed to α phase based on the micro twins observed in α during TEM examination (Figure 3a).

Lu et al. [22] have recently provided an alternate pathway for the formation of α in EBM Ti64. They showed the presence of massive α_m in as-fabricated samples in their study. According to them, the transformation on cooling from β phase is a mix of α' and α_m formation. The α_m then decomposes to acicular α during the prolonged hold time at elevated temperature during the EBM process. The presence of larger size patchy massive α_m on top of the build compared to regions of extremely fine acicular α at the bottom was concluded to be indicative of the dynamic nature of these decomposition reactions. However, a cooling rate in the range 20-410$\frac{K}{s}$ from the β phase field was used to justify the existence of α' and α_m at the same time [22]. They identified four types of α_m based on its nucleation site in β grains, the details of which can be found in their work.

Similar to Ti64, IN718 has been widely fabricated using various AM processes. However, unlike the simpler two-phase α/β Ti64 microstructure, IN718 has the ability to precipitate a large number of phases as a function of time and temperature [3]. In their work of IN718 fabricated through LENS, Tian et al. [23] observed the formation of Nb-rich (Ni_3Nb-γ") precipitates in the earliest material laid, whereas, the last material deposited contained higher amounts of metastable products (Laves and NbC) within the interdenritic regions. With this, Tian et al. [23] reported a sensitivity of the hardness response to be associated with the heterogeneous microstructure along the build direction. Ultimately it was theorized the formation of the γ" being associated with the continuous thermal gyrations caused by layer addition and the higher degree of elemental segregation due to the high solidification rates. Interestingly though, studies for IN718 fabricated through SLM have not indicated the presence of a heterogeneous microstructure as seen in LENS [24, 25].

Similarly, in their work on EBM IN718, Kirka et al. [26] described a spatially varying microstructure that was classified into three regions as illustrated in Figure 4. At the top surface was reported a refined dendritic structure (7 μm primary dendrite arm spacing) with Laves and MC carbides within the interdendritic region and γ" within the matrix that precipitated upon cooling of the build. With increasing distance away from the top surface, the dendritic structure was observed to become diffuse in nature, dissolution of the Laves phase as a result of thermal exposure, and precipitation of δ having begun in Nb-rich interdenritic regions previously occupied by the Laves. Further, within the bulk and with the material's assumption of the EBM background temperature ($\approx 900^{\circ}$C), the metastable strengthening γ" was observed to increasingly decompose and form networks of zipper-like δ across entire grains with the remaining γ" coarsening beyond the peak size for optimal mechanical performance.

Aside from microstructure heterogeneities within EBM material, δ precipitate morphologies and struc-

tures have been shown sensitive to the background temperature of the build. Morphologies range from networks of fine zipper-like and globular δ, to large needle-like δ that span entire grains [26–28]. The morphological evolution of δ in traditionally processed IN718 is directly related to the thermal conditions at which the material is held [29]. The combined observations of microstructure heterogeneity and phase morphology sensitivity to time and temperature highlight the need for enhanced understanding of engineering alloys processed through AM techniques and need for process-structure properties such that the microstructure is a known quantity.

Much has been reported to date on rationalizing both the solidification phenomena and solid-solid phase transformations in metals AM, however, this has occurred in a disjointed manner between experiments and modeling efforts. From the standpoint of solidification modeling, the effects of thermal gyrations associated with multiple tracks in a single layer or a single track spanning many layers are not sufficient to understand the multidimensional influence on the $l \rightarrow S$ and $S \rightarrow S$ phase transformations under geometric complex relevant conditions. Whereas in experimental studies, more complex heat source fills such as island and point fill have been implemented to influence thermal conditions within the material. However, owing to the huge computational costs, modeling efforts have been limited to single melt tracks and rectangular melt areas lacking the resemblance of relevant geometries fabricated by AM. Lastly, to fully leverage the promise of site-specific microstructures within material, advanced knowledge of both the local and macro thermal states of the material during processing is required.

In the case of solid-solid phase transformations such as Ti64, there is no clear consensus on the mechanism of phase transformations for like AM processes. The lack of consensus is potentially associated with the assumed cooling rate vs the true cooling rate of the material and ultimate sensitivity of the microstructure to process parameters. Additionally, for IN718, the occurrence of thermal gyrations in AM processes makes it nearly impossible to currently predict their formation and dissolution over full scale engineering components.

Currently, metals AM is at an inflection whereby AM processes have the capability to fabricate complex geometries, however, lack the level of understanding and insight into comparable materials fabricated through forging and castings. If AM is to rise to similar levels, a coordinated alignment between experimental and modeling efforts is required such that current solidification and phase transformation models can be validated with highly pedigreed data sets to evaluate their capabilities. In the future, a concentrated effort must occur whereby the AM community develops computationally efficient multi-scale [30] models that have the ability to simulate the entirety of an AM build that is comprised of relevant complex geometries. Lastly as a grand challenge, an emphasis must be placed on developing the abilities to solve inverse problems. That is where the resultant texture and microstructure is known in a spatial domain, and it is the process parameters and build conditions that give rise to the desired

structure that are determined and then used as inputs into the actual AM build process.

In the present discussion, the current efforts and understanding of both $l \rightarrow S$ and $S \rightarrow S$ phase transformations in Ti64 and IN718 have been discussed. Compared to their traditional counterparts, phase transformations in AM processed materials are more complex due to the high cooling rates, thermal gyrations, and spatially dependent microstructures. While the underlying physics of AM processes are very much similar to traditional welding, no thermal and kinetics models currently exist that have the ability to capture the coupled rapid thermal cycling and resultant phase transformations AM materials undergo in full scale components. In the future, as AM materials become utilized for ever critical engineering applications, a complete understanding of the physical process and materials will be needed.

1 Acknowledgements

This research sponsored by the US Department of Energy, Office of Energy Efficiency and Renewable Energy, Advanced Manufacturing Office, under contract DE-AC05-00OR22725 with UT-Battelle, LLC.

2 References

[1] Gibson, I., Rosen, D. W., Stucker, B., et al., 2010. *Additive manufacturing technologies*. Springer.

[2] Ahmed, T., and Rack, H., 1998. "*Phase transformations during cooling in + titanium alloys*". *Materials Science and Engineering: A,* **243**(1–2), pp. 206 – 211.

[3] Sims, C., 1972. *The Superalloys*. John Wiley and Sons.

[4] Andersson, J., and Sjöberg, G. P., 2012. "*Repair welding of wrought superalloys: Alloy 718, Allvac 718Plus and Waspaloy*". *Science and Technology of Welding and Joining,* **17**(1), pp. 49–59.

[5] Hussein, A., Hao, L., Yan, C., and Everson, R., 2013. "*Finite element simulation of the temperature and stress fields in single layers built without-support in selective laser melting*". *Materials & Design,* **52**, pp. 638 – 647.

[6] Manvatkar, V., De, A., and DebRoy, T., 2015. "*Spatial variation of melt pool geometry, peak temperature and solidification parameters during laser assisted additive manufacturing process*". *Materials Science and Technology,* **31**(8), pp. 924–930.

[7] Wei, H. L., Mazumder, J., and DebRoy, T., 2015. "*Evolution of solidification texture during additive manufacturing*". *Scientific Reports,* **5**, 11, pp. 16446 EP –.

[8] Helmer, H., Bauereiß, A., Singer, R. F., and Körner, C., 2016. "*Grain structure evolution in Inconel 718 during selective electron beam melting*". *Materials Science and Engineering: A,* **668**, 6, pp. 180–187.

[9] Raghavan, N., Dehoff, R., Pannala, S., Simunovic, S., Kirka, M., Turner, J., Carlson, N., and Babu, S. S., 2016. "*Numerical modeling of heat-transfer and the influence of process parameters on tailoring the grain morphology of {IN718} in electron beam additive manufacturing*". *Acta Materialia,* **112**, pp. 303 – 314.

[10] Dinda, G., Dasgupta, A., and Mazumder, J., 2012. "*Texture Control During Laser Deposition of Nickel-based Superalloy*". *Scripta Materialia,* **67**, pp. 503–506.

[11] Dehoff, R. R., Kirka, M. M., Sames, W. J., Bilheux, H., Tremsin, A. S., Lowe, L. E., and Babu, S. S., 2015. "*Site specific control of crystallographic grain orientation through electron beam additive manufacturing*". *Materials Science and Technology,* **31**(8), pp. 931–938.

[12] Kobryn, P., and Semiatin, S., 2001. "*The laser additive manufacture of Ti-6Al-4V*". *JOM,* **53**(9), pp. 40–42.

[13] Kobryn, P., and Semiatin, S., 2001. "*Mechanical Properties of Laser-Deposited Ti-6Al-4V*". In Solid Freeform Fabrication Symposium, pp. 179–187.

[14] Kelly, S. M., and Kampe, S. L., 2004. "*Microstructural evolution in laser-deposited multilayer Ti-6Al-4V builds: Part I. Microstructural characterization*". *Metallurgical and Materials Transactions A,* **35**(6), pp. 1861–1867.

[15] Sridharan, N., Chaudhary, A., Nandwana, P., and Babu, S. S., 2016. "*Texture Evolution During Laser Direct Metal Deposition of Ti-6Al-4V*". *JOM,* **68**(3), pp. 772–777.

[16] Simonelli, M., Tse, Y. Y., and Tuck, C., 2014. "*On the Texture Formation of Selective Laser Melted Ti-6Al-4V*". *Metallurgical and Materials Transactions A,* **45**(6), pp. 2863–2872.

[17] Thijs, L., Verhaeghe, F., Craeghs, T., Humbeeck, J. V., and Kruth, J.-P., 2010. "*A study of the microstructural evolution during selective laser melting of Ti–6Al–4V*". *Acta Materialia,* **58**(9), pp. 3303 – 3312.

[18] Xu, W., Brandt, M., Sun, S., Elambasseril, J., Liu, Q., Latham, K., Xia, K., and Qian, M., 2015. "*Additive manufacturing of strong and ductile Ti–6Al–4V by selective laser melting via in situ martensite decomposition*". *Acta Materialia,* **85**, pp. 74 – 84.

[19] Al-Bermani, S., Blackmore, M., Zhang, W., and Todd, I., 2010. "*The Origin of Microstructural Diversity, Texture, and Mechanical Properties in Electron Beam Melted Ti-6Al-4V*". *Metallurgical and Materials Transactions A,* **41**(13), pp. 3422–3434.

[20] Tan, X., Kok, Y., Tan, Y. J., Descoins, M., Mangelinck, D., Tor, S. B., Leong, K. F., and Chua, C. K., 2015. "*Graded microstructure and mechanical properties of additive manufactured Ti–6Al–4V via electron beam melting*". *Acta Materialia,* **97**, pp. 1 – 16.

[21] Banerjee, D., Shelton, C., Ralph, B., and Williams, J., 1988. "*A resolution of the interface phase problem in titanium alloys*". *Acta Metallurgica,* **36**(1), pp. 125 – 141.

[22] Lu, S., Qian, M., Tang, H., Yan, M., Wang, J., and StJohn, D., 2016. "*Massive transformation in Ti–6Al–4V additively manufactured by selective electron beam melting*". *Acta Materialia,* **104**, pp. 303 – 311.

[23] Tian, Y., McAllister, D., Colijn, H., Mills, M., Farson, D., Nordin, M., and Babu, S., 2014. "*Rationalization of Microstructure Heterogeneity in INCONEL 718 Builds Made by the Direct Laser Additive Manufacturing Process*". *Metallurgical and Materials Transactions A,* **45**(10), pp. 4470–4483.

[24] Strößner, J., Terock, M., and Glatzel, U., 2015. "*Mechanical and Microstructural Investigation of Nickel-Based Superalloy IN718 Manufactured by Selective Laser Melting (SLM)*". *Advanced Engineering Materials,* **17**(8), pp. 1099–1105.

[25] Amato, K., Gaytan, S., Murr, L., Martinez, E., Shindo, P., Hernandez, J., Collins, S., and Medina, F., 2012. "*Microstructures and mechanical behavior of Inconel 718 fabricated by selective laser melting*". *Acta Materialia,* **60**(5), pp. 2229 – 2239.

[26] Kirka, M. M., Unocic, K., Raghavan, N., Medina, F., Dehoff, R. R., and Babu, S. S., 2016. "*Microstructure Development in Electron Beam Melted Inconel 718 and Associated Tensile Properties*". *Journal of Materials.*

[27] Unocic, K. A., Kolbus, L. M., Dehoff, R. R., Dryepondt, S. N., and Pint, B. A., 2014. "*High Temperature Performance of UNS N07718 Processed by Additive Manufacturing*". In Corrosion, NACE International.

[28] Strondl, A., Palm, M., Gnauk, J., and Frommeyer, G., 2011. "*Microstructure and mechanical properties of nickel based superalloy IN718 produced by rapid prototyping with electron beam melting (EBM)*". *Materials Science and Technology,* **27**(5), pp. 876–883.

[29] Carlson, R., and Radavich, J., 1989. "*Microstructural Chraterization of Cast 718*". In Superalloy 718: metallurgy and applications, E. Loria, ed., Minerals, Metals & Materials Society, pp. 79–95.

[30] King, W., Anderson, A. T., Ferencz, R. M., Hodge, N. E., Kamath, C., and Khairallah, S. A., 2015. "*Overview of modelling and simulation of metal powder bed fusion process at Lawrence Livermore National Laboratory*". *Materials Science and Technology,* **31**(8), 06, pp. 957–968.

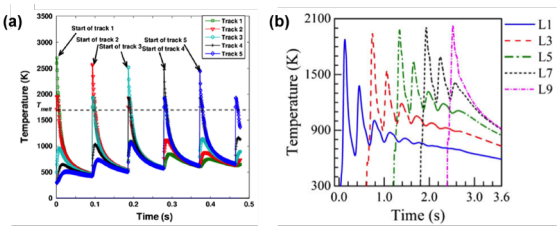

Figure 1: Thermal cycles (a) multiple tracks on a single layer adapted from [5] and (b) multiple layers on a single track adapted from [6].

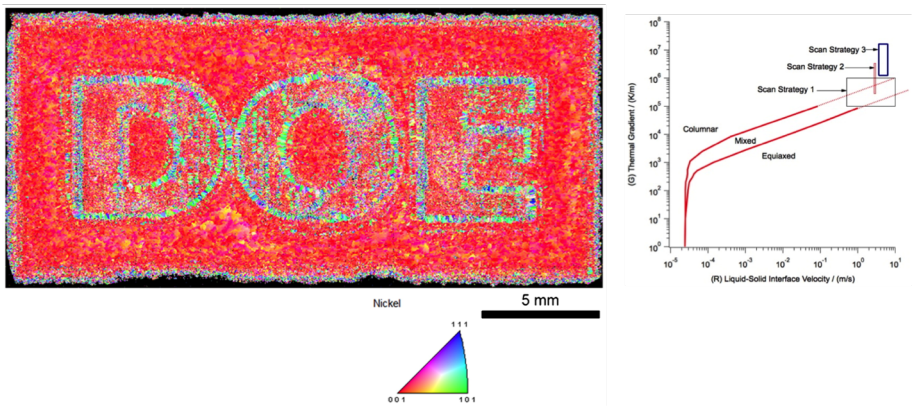

Figure 2: Crystallographic orientation map corresponding to inverse pole figure for fcc nickel obtained on cross-section of EBM build obtained through EBSD: The bulk shows $\langle 001 \rangle$ columnar solidification grain growth, the outline of the letters show equiaxed grain growth indicated by lack of any significant $\langle 001 \rangle$ component, and the interior areas of letters D, O and E exhibit a mixture of $\langle 001 \rangle$ growth with the solidification map for Inconel 718 describing the estimated ranges for G and R for each of scan strategies overlaid. Adapted from [11].

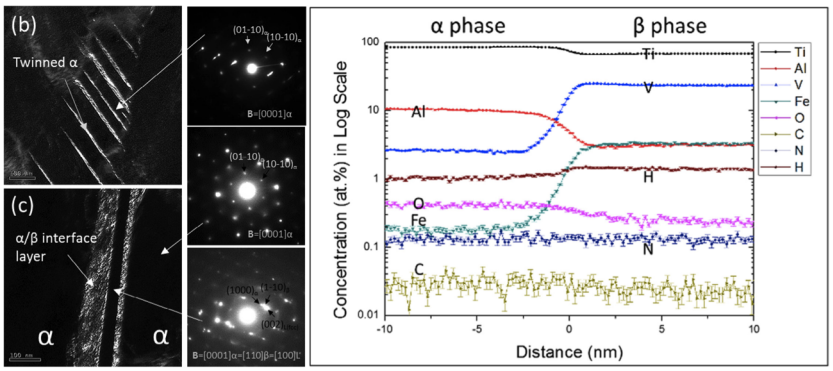

Figure 3: (a) twinned α indicating the transformation from prior α' with the corresponding SAED from (0001) in inset, (b) α/β interface layer along with the corresponding SAEDs in inset with the bottom inset showing the FCC reflections, and (c) the composition profile across the α/β interface showing the absence of a hydride phase during atom probe analysis. Adapted from [26].

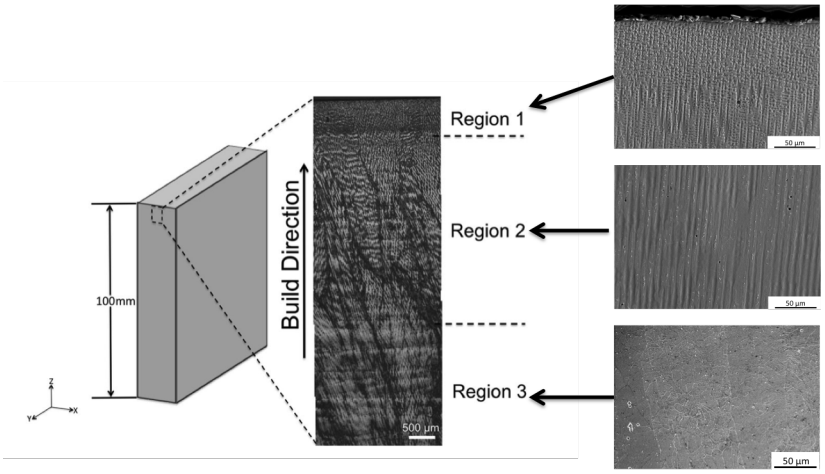

Figure 4: Optical micrograph depicting the tri-zone spatially dependent microstructure observed within EBM IN718 with detailed SEM images depicting the local microstructures. Region 1: Dendritic structure spanning the last few layers fo the build. Region 2: Diffuse dendritic structure. Region 3: Precipitation of δ within the matrix. Adapted from [26].